JP&M Engineering
Journal of Petroleum and Mining Engineering

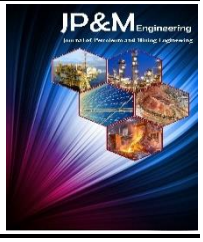

Processing and Characterization of Geopolymer Based on Ladle Furnace Slag and Fly Ash: the Impact of Chemical Composition on the Biodiesel Production

Mennatallah S. Barbarey [*a,b], Mohamed M. E. Seleman[a], Amany A. El Kheshen[c], Mahmoud F. Zawrah[d,e]
[a] Department of Metallurgical and Materials Engineering, Faculty of Petroleum and Mining Engineering, Suez University, Suez 43221, Egypt
[b] Canal High Institute of Engineering and Technology, Suez 43512, Egypt
[c] Glass Research Departments, National Research Centre, 12622 Dokki, Cairo, Egypt
[d] Refractories, Ceramics and Building Materials Department, National Research Centre, 12622 Dokki, Cairo, Egypt
[e] Pharos University in Alexandria, Smoha, Alexandria, Egypt
*Corresponding author e-mail: mennatallah.bafa@pme.suezuni.edu.eg

Article Info

Received 6 May 2024
Revised 15 Jun. 2024
Accepted 28 Jun. 2024

Keywords

"Geopolymers; Ladle slag; Flay ash, Catalyst; Biodiesel"

Abstract

The goal of the present study was to produce geopolymers based on flay ash and recycled ladle furnace slag as starting materials. This aim was extended to study the applicability of using these geopolymers as a catalyst for the production of biodiesel. Geopolymers were prepared in multiple batches using fly ash and ladle slag in the presence of an alkali solution. X-ray diffraction (XRD) and Fourier Transform Infrared Spectroscopy (FT-IR) were used to assess the phase identification of the manufactured geopolymers. The apparent porosity and bulk density as physical properties of the processed materials were evaluated. In addition, a compressive strength test was conducted. A trial was carried out utilizing the calcined geopolymer powders at varying temperatures (110-700 ^{o}C), as a catalyst in the production of biodiesel. This process was achieved in the presence of soybean oil and methanol. The kinetic viscosity, flash point, and density of the prepared biodiesel were measured to assess its efficiency. The gained results showed that ladle slag and fly ash could be effectively used to manufacture geopolymer bulk materials. The density and compressive strength of the prepared geopolymers were improved by increasing the fly ash content in the batches. The batch containing 30% fly ash and 70% slag exhibited the highest compressive strength (14.5 MPa) of the developed geopolymers. In addition, the generated biodiesel's viscosity, flash point and density measurements fell within the expected ranges of 2.8-5.1 mm^2/s, 90-135 °C and 0.848-0.885 g/cm^3, respectively.

Introduction

Cement is regarded as a typical building component. Currently, the annual global consumption of ordinary Portland cement (OPC) is projected to reach 4.1 billion tones in 2022. In 1995, the total volume of cement production was just 1.39 billion tons, indicating an increase in the construction industry. The principal greenhouse gas released during cement manufacturing as one main byproduct is CO_2. It contributes approximately 7% of the CO_2 input to the atmosphere overall. In general, OPC manufacturing is a very polluting, high-temperature, and energy-consuming process [1,2]. Owing to these conditions, researchers are now looking at cheaper and more environmentally friendly building materials with excellent compressive strength. Currently, geopolymer cement is considered a new building material under research. The fact that geopolymers are manufactured from industrial waste as raw materials and have a more environmentally friendly manufacturing process than OPC is a significant advantage. Geopolymers are ceramic-like amorphous inorganic polymers that can be synthesized via solid aluminosilicate polycondensation in a highly alkaline medium through geopolymerization below 100 °C [3]. They are formed by networks or chains of covalently bonded mineral molecules. Because they are polymers, they should be discussed using vocabulary specific to polymers rather than the conventional nomenclature employed by ceramicists.

In recent years, geopolymers and their composites have received considerable attention owing to their distinct and beneficial performance [4]. These materials combine some desirable properties owing to their characteristics of cements and inorganic polymers, including low energy consumption, low CO_2 emissions compared to (OPC), acid resistance, thermal stability, chemical stability, high mechanical properties, and good thermal

resistance [5]. Nowadays, they are used in a wide series of various applications owing to their different properties for medicinal applications, radioactive and toxic waste control, cementitious and construction materials, advanced binders, high-temperature resistant ceramics, fire protection, heat-resistant coatings, optical applications, and catalytic materials [6-9].

Geopolymer production utilizes waste materials and manufacturing byproducts rich in alumina and silica, such as waste glass powder, ground granulate blast furnace slag (GGBS), ferrochrome ash, metakaolin (MK), and fly ash (FA), as well as waste agriculture, such as rice husk ash and sugarcane bagasse [10-13]. The compressive strength is increased when NaOH and commercial Na_2SiO_3 solutions are utilized as activators in the company of fly ash and pulverized granulated slag of blast furnaces as the supply materials [14,15]. Fly ash, a byproduct of burning coal, is now utilized to synthesize geopolymer materials because of its high silica and alumina content. Recently, FA has frequently exhibited significant levels of lime and sulfite owing to changes in raw coal and coal-burning technologies [16]. Chen et al. indicated that the mechanical properties of geopolymers based on fly ash first increased and then decreased with increasing sulfite and lime content. According to the findings, the created geopolymers had the best qualities at 20°C when the sulfite and lime contents were 4% and 11%, respectively. The increases in flexural strength and compressive strength at 28 days after demolding were 15.56% and 17.91%, respectively. The reduction in drying shrinkage was 60.65% [17]. According to research, fly ash, slag, building waste, and other low-energy-consumption industrial wastes can be employed as raw materials for geopolymer manufacturing, which can save more than 75% of energy and reduce emissions by more than 95% [18-20]. Recent studies have indicated that fly ash or slag can be used in concrete as a binder through the process of polymerization as activators with alkali components. Through the geopolymer reaction, the formation of the inorganic binder is due to the activation of fly ash as a source of aluminates and silicates in a highly alkaline solution. The production of calcium silicate hydrate gel (C-S-H gel), as created in OPC, is caused by the activation of slag as a source of calcium and silicates. Arie et al. investigated the ability of alkali-activated slag/fly ash mortar blends at a suitable temperature to substitute OPC in concrete to reduce the environmental influence on CO_2 evolution. The results indicated that the best strength results were produced by combining the percentage of 0.5 slag to 0.5 fly ash, and by increasing the fly ash content, the values of the standard deviation improving the stability of the specimen were reduced. It is also recommended that a 0.5 fly ash blend with 0.5 slag could supply a solution to the heat preservation requirement for geopolymers based on fly ash [21].

Owing to their catalytic properties, geopolymers, such as aluminosilicate-based ceramics [22], are applied as heterogeneous catalysts for the production of biodiesel. Recently, heterogeneous catalysis has been considered green chemistry because it allows for faster mechanical separation of products, thereby substituting conventional unit procedures that consume energy (such as distillation) or generate waste (such as solvent extraction) [23]. One of the many challenges faced by green chemistry is the use of solid catalysts to convert animal fats and vegetable oils to short-chain alcohols to produce biodiesel as ethyl or methyl esters [24-28].

The aim of this study was to produce geopolymers as binding materials using ladle furnace slag waste slag and fly ash (FA). Additionally, it is challenging to use the produced geopolymers as heterogeneous catalysts for the production of biodiesel. Enhanced properties were obtained by using an appropriate amount of slag. The produced geopolymers were evaluated as biodiesel catalysts, and their physical properties, including compressive strength, were evaluated.

Experimental Method

Initial materials

The present investigation utilized water-cooled ladle furnace slag sourced from the slag yard at the Ezz flat steel company, situated in the Suez governorate of Egypt. Initially, the slag was pulverized for a period of three hours using a laboratory ball mill, resulting in the production of a fine powder with a specific gravity of approximately 3000 kg/m^3 and a surface area of approximately 610 m2 kg^{-1}.

On the other hand, low calcium fly ash (class F: according to ASTM C 618) [29] and high silicate (SiO_2) content were applied as primary raw materials. The fly ash used had a (SiO_2 + Al_2O_3 + Fe_2O_3) content of 88.01%, which is less than 70%; a CaO content of 2.62%, which is greater than 10%; and a composition of 1.93% SO_3 according to ASTM C618 [30]. The chemical composition of the sodium silicate solution, which was purchased from Fisher Scientific Company in the UK, was 30.1% SiO_2, 9.4% Na_2O, and 60.5% H_2O (silicate modulus, SiO_2/Na_2O = 3.2). Its density at 20°C was 1500 Kg/m^3. Additionally, Sigma-Aldrich Co., USA, provided NaOH pellets (98% purity).

Geopolymers preparation

Initially, the sodium silicate solution and 10 M (molarity) NaOH solution were combined in a 1:1 ratio to create the alkali activator solution, which was then left to settle until it was transparent. This solution was prepared at least 24 h prior to the production of pastes to allow it to reach equilibrium. A ball mill was employed to blend, mix, and homogenize a multitude of ladle furnace slag (LFS) and fly ash batches for 30 min, as outlined in Table 1.

Table 1 Studied geopolymer batches.

Sample No.	F0	F10	F20	F25	F30
Fly Ash (FA)	0	10	20	25	30
Ladle furnace slag (LFS)	100	90	80	75	70

The addition of the desired alkali activator solution to the planned mixes was determined based on the proportions of the mixed elements. The mixing process was completed by vigorously mixing the mixture continuously for 10 min by hand to ensure good adhesion among the ingredients. The fresh mixture pastes were placed into plastic cube molds with dimensions of approximately 2.5 cm x 2.5 cm x 2 cm for length, width, and height, respectively. The molds were then vibrated on a vibrating table for approximately 1-2 minutes to eliminate any air bubbles and create a more compact paste.

A thin-edged trowel was used to smoothen the paste surface. The molds were then placed inside a humidity chamber at a constant temperature of 23 ±2 °C and 100% relative humidity. The molds were covered with a thin plastic film to prevent excessive moisture loss for the first 24 h. After demolding, the synthesized cubes were maintained at room temperature for 28 days after demolding. Each sample was then dry-cured under ambient laboratory conditions at atmospheric pressure, with no effort made to control the humidity during the curing process.

Characterization of initial materials and fabricated geopolymers

Using a Bruker S4 X-ray fluorescence model, which was imported from Germany and came with a Rh source and a 2.2 KW power tube, the chemical composition of LFS and fly ash was examined. The mineralogical phase compositions of the ingredients and resulting geopolymers were determined using a Siemens D5000 powder diffractometer operating at 40 kV and 30 mA with Cu-K radiation (wavelength = 0.15406 nm). The diffractometer was set to a step size of 0.02° and step step-time of one second within the range of $10 < 2\theta < 100$. The XRD patterns of the produced samples were compared with the ICDD (JCPDS) standard cards. To verify the composition and determine the functional groups of the ingredients and fabricated geopolymers, FTIR was used in conjunction with FT/IR-ATR-Wistar-Alpha. Spectra were recorded between 400 and 4000 cm^{-1} at a resolution of 4 cm^{-1} at 25°C.

Three sets of each mix were examined for bulk density, apparent porosity, and compressive strength in accordance with the guidelines set forth by ASTM C 20=2000 and ASTM C109. The water displacement method was used to determine the density and apparent porosity in accordance with Archimedes' principle. The compressive strength was assessed using an automatic testing machine with a load capacity of 1000 KN and a rate of 0.025 KN/mm^2/s. Additionally, the microstructure of the generated geopolymers was investigated using EDX equipment in conjunction with scanning electron microscopy (SEM-JEOL Ltd., Japan).

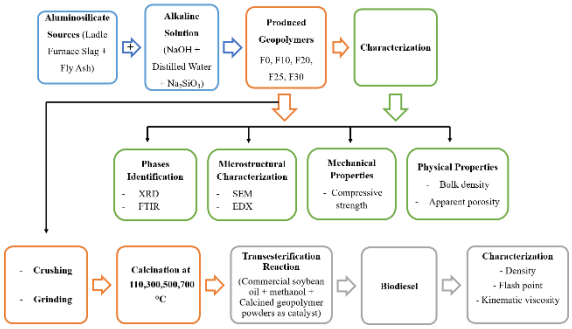

Figure 1 Chart diagram describing the experimental procedure.

To use the fabricated geopolymer as a catalyst in the production of biodiesel, the following steps have been done. After milling into fine powders, the geopolymer samples were heated to a range of temperatures, including 110, 300, 500, and 700 °C. Commercial soybean oil and methanol were used in a transesterification reaction to produce biodiesel. To ensure that all the methanol in the flask was forced to reflux, the reaction was conducted in a 100 ml flask that was vigorously stirred and connected beneath a vertical condenser with cold water. For transesterification, a molar ratio of 7.5:1 was used with a catalyst concentration of 3%. For each sample, the reaction time was 4 h. The mixture was cooled once the reaction was complete, and the generated phases (catalyst, biodiesel, and glycerol) were separated using centrifugation. To remove the extra methanol, the separated biodiesel phase was heated to 100°C and evaporated. The density, flash point, and kinematic viscosity of the produced biodiesel were measured to evaluate its efficiency. Viscosity and density measurements were performed using the Stabinger SVM 3000 model of the Anton Paar apparatus. The average of triplicate measurements was used to record the data. The SYD-3536 tester calculated the flash point according to ASTM-D93.

Results and Discussion

Evaluation of the starting materials

As analysed by XRF, the chemical compositions of both the fly ash and ladle furnace slag are listed in Table 2. As can be observed, SiO_2 and Al_2O_3 are the main components of fly ash, along with a few additional minor oxide impurities. In contrast, LFS waste contains primarily SiO_2, Al_2O_3, MgO, and CaO along with a few other minor oxides. SiO_2 and Al_2O_3 were present in lesser amounts than CaO or MgO, indicating a greater basic character (2.14).

The XRD pattern of the LFS (Figure 2) shows that it consists of calcium aluminum oxide ($Ca_{12}Al_{14}O_{33}$), calcium aluminosilicate ($Ca_2Al_2SiO_7$), dicalcium silicate (Ca_2SiO_4), and magnesium oxide (MgO) phases as impurities. Figure 3 illustrates the XRD pattern of the fly ash. It is shown that the mullite and quartz phases were the two major phases and a small amount of hematite phase.

Table 2 Chemical composition of FA and LFS in mass, %

Composition	FA	LFS
Al_2O_3	27.83	4.09
Na_2O	1.13	0.02
MgO	1.43	6.62
CaO	2.62	58.23
SiO_2	50.97	26.27
Fe_2O_3	9.21	1.69
TiO_2	1.15	0.44
K_2O	3.73	0.01
MNO	---	0.85
SO_3	1.93	---

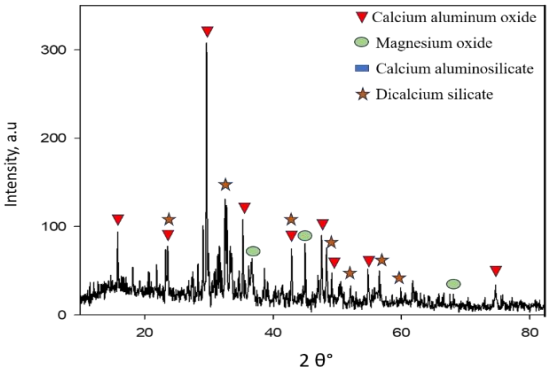

Figure 2 XRD pattern of ladle furnace slag.

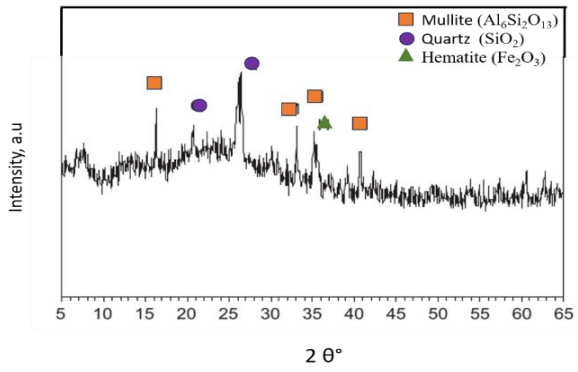

Figure 3 XRD pattern of fly ash.

Figure 4 shows the FTIR spectra of LFS, which reveal a broad band at 3723 cm^{-1} attributed to the vibration of OH groups in response to adsorbed water. The Mg-O vibration bond of magnesia is represented by bands located at 2358 and 1585 cm^{-1}, whereas the Al-O bond of calcium aluminates or calcium aluminum silicate is responsible for the band at 663 cm^{-1}. The Si-O silicate band is indicated by the band at 423 cm^{-1}. The FTIR spectra of fly ash is shown in Figure 5, which reveals that –OH stretching and H-O-H bending vibrations of bound water molecules, trapped in polymeric framework cavities and absorbed on the surface, are indicated by the band area 3500-1600 cm^{-1}. The Si-O-Si bands characteristic of quartz are indicated by the band area 1600-1000 cm^{-1}, while the symmetric stretching of Si-O-Si and Al-O-Si bonds, describing the creation of an amorphous to semi-crystalline alumino-silicate materials, is specified by the band area 800-500 cm^{-1}. Bands below 500 cm^{-1} are characteristic of the bending vibrations of Si–O–Si and O-Si-O bonds.

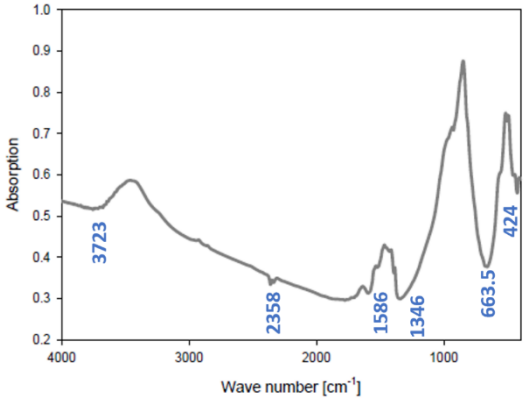

Figure 4 Fourier transmission IR spectrum of ladle furnace slag.

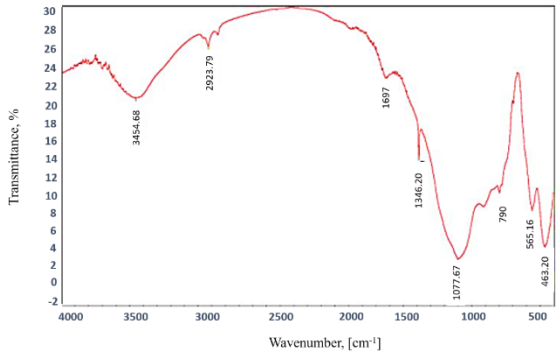

Figure 5 FTIR spectrum of fly ash.

Geopolymers characterization

Physical properties of fabricated geopolymers

According to various studies, the concentration and type of alkali activator, size of the starting powder particle, solid/liquid ratio, temperature at which the casted pastes cure, and chemical composition of the starting materials are the primary factors that influence the physical properties of geopolymers [31-33]. The apparent porosity (AP) and bulk density (BD) of the slag-fly ash geopolymers are displayed in Figure 6. As can be observed in Figures 6a, the bulk density decreases from 1.93 to 1.82 g/cm^3 when the amount of fly ash added to the geopolymer increases. This decrease in bulk density is attributed to the fact that the oxides of ladle slag have a higher density than fly ash. Furthermore, micro-and nanopores are present in the resulting structures owing to the development of hydrated components such as sodium aluminum silicate hydrate (NASH), calcium aluminum silicate hydrate (CASH) and calcium silicate hydrate (CSH). This is evident in Figure 6b, which shows that the porosity increased with the addition of up to 30% fly ash.

XRD pattern of produced geopolymers

In this study, the starting materials used for producing geopolymers were silica-alumina-rich fly ash and calcium oxide-silica-rich slag. Therefore, it is expected that batches high in fly ash will form a NASH gel structure with a Na_2O-Al_2O_3-SiO_2-H_2O structure, whereas batches rich in slag will produce a CSH phase [34,35]. Additionally, intermediate batches possess the capacity to produce CSH and CASH phases. Figure 7 shows The XRD patterns of the produced

geopolymers. It is important to note in this research that the reaction of slag, fly ash, and sodium silicate activator produces phases that range from amorphous to partially crystalline. A poorly crystalline phase [C-A-S-H] was identified as the primary phase. The batch F0, which includes 100% LFS, demonstrates CSH as the chief phase. The broad peak at 2 Theta, which ranges from 20° to 40°, indicates that the geopolymer is mainly amorphous. Numerous studies have demonstrated that the produced C-A-S-H lamellar structure in alkali activated slag strongly resembles that of tobermorite [36-38]. In the dreierketten silicate chains, Al^{3+} in C-A-S-H replaces Si^{4+}, which is charged equally by alkali or Ca^{2+} cations [36]. In the case of N-A-S-H, alkaline cations (such as Na+) balance out the charge balance associated with Al3+, while Si4+ and Al3+ are organized in tetrahedral shapes to make 3D structures. Furthermore, N-A-S-H has a variable Al/Si ratio that normally falls between 0.28 and 0.36 [40]. It is established that the production of NASH gel with good mechanical characteristics occurs when FA is activated by NaOH in the presence of a sodium silicate solution, whereas when FA is present, as in the case of the F25 and F30 samples, the alkali activation of LFS speeds up the geopolymerization process and creates new phases that could assist the geopolymer-gel gain strength. Prior research has demonstrated the presence of geopolymeric gels and CSH/CASH (NASH and NCASH) in various batches containing slag or calcium hydroxide as calcium sources [41].

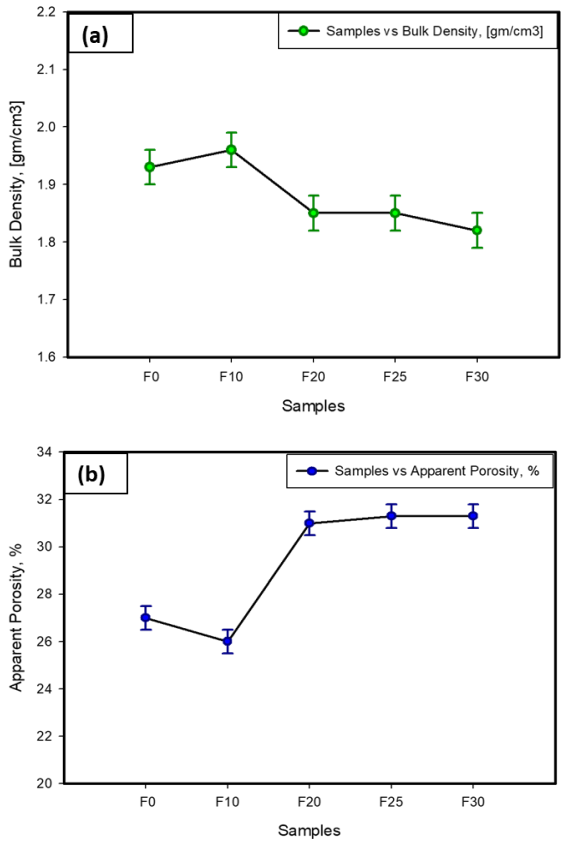

Figure 6 The bulk density of studied geopolymers cured in air for 4 weeks (a) and the apparent porosity of synthesized geopolymers cured in air for 4 weeks (b) produced at different 100% to 70% LFS.

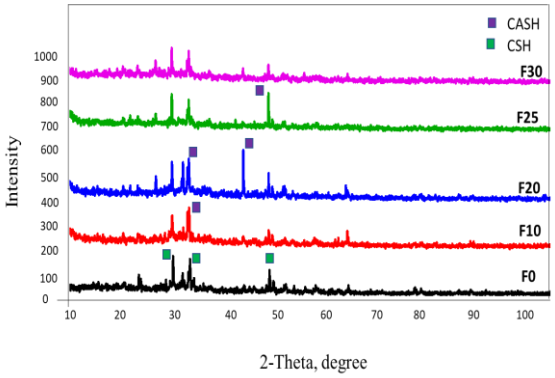

Figure 7 XRD patterns of studied geopolymers cured in air for 4 weeks.

FTIR of produced geopolymer

Figure 8 shows FTIR spectra of the produced geopolymer after four weeks of curing. Regarding the bending and stretching of the OH group, small and wide bands were observed at 3400–3470 and 1420 cm^{-1}, respectively. When more fly ash is introduced, their intensities increase slightly, resulting in the production of geopolymer phases (NASH, NCASH). These bands are ascribed to H_2O molecules that have been adsorbed or cached in large spaces in the geopolymeric skeleton connected to the reaction products [42,43]. The band at 1409–1439 cm^{-1} was ascribed to O–C–O bond stretching vibrations, indicating the presence of CO_3^{-2} produced as a result of ambient carbon dioxide [44]. This band becomes smaller as more geopolymer phases emerge, or as the phases that are rich in calcium and insatiable for carbonation become smaller.

A significant concentration of Na_2CO_3 can impede the progress of geopolymerization. T represents the tetrahedrons of Si or Al, and the asymmetric stretching vibration of the Si–O–T bonds is responsible for the prominent band at 958–990 cm^{-1}. The addition of more fly ash led to a higher degree of geopolymerization, resulting in the formation of a strongly cross-linked geopolymer gel framework. As the geopolymerization process concludes, the band that signifies this phenomenon shifts slightly to a lower wave number (958–990 cm^{-1}). This shift may be attributed to the partial substitution of tetrahedral aluminium (AlO_4) with tetrahedral silicon (SiO_4). The resulting aluminosilicate gel alters the chemical structures surrounding the Si–O bond.

After polymerization, the band at 790 cm^{-1}, which corresponds to pure fly ash, and the Al-O and Si-O bending shifts to a higher wavenumber (950 cm^{-1}). This suggests that increased concentrations of AlO_4 were formed during the disintegration of fly ash [45,46]. Only batches with higher amounts of FA exhibit a short band between 851 and 863 cm^{-1}, which is attributed to the symmetric stretching vibrations of Si–O–Si (Al) bridges. Conversely, the band at 865 cm^{-1} was ascribed to the symmetric stretching of Al–O–Si, whereas the band at 436 cm^{-1} related to the bending of Si–O–Si and O–Si–O bonds [47].

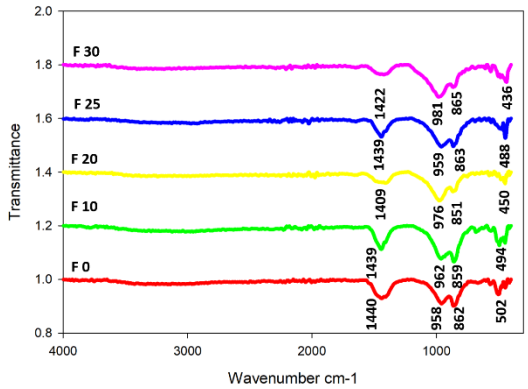

Figure 8 The FT-IR spectra of the geopolymers that were produced and cured in air for one week.

Microstructure of produced geopolymer

Figures 9, 10, and 11 show the EDAX analysis and SEM micrographs of geopolymers F0, F10, and F30, respectively. Significant variations in the microstructures of the generated geopolymers were noted. Large gaps between coarse, well-crystalline grains characterize the geopolymer made entirely of slag (F0). Since most of the grains are large and coarse, there are not many tiny pores found in the microstructure. These large grains had outlines of small, distorted grains with coarse edges. EDAX examination of these grains indicated that they were high in calcium. These phases consist of trace amounts of CASH, NCASH, and magnesium silicate hydrate (MSH) along with CSH and/or NCSH. On the surfaces of the main phases (CSH, NCSH, or both), CASH grains appear as long plate nanograins or fiber-like particles. Conversely, the F10 geopolymer, which is made up of 90% slag and 10% FA, has a microstructure that is comparable to that of the F0 geopolymer, but with more grain growth. There were large, clumped coarser granules in the microstructure. This microstructure also exhibited indications of large voids. Some geopolymer gels were formed in this sample once 10% FA was added. The development of tiny gaps between the gels is favored by the establishment of geopolymer networks. As evidenced by the apparent porosity results (Figure. 6b), this sample has a larger porosity than the sample made entirely of slag because it has large voids as well as tiny pores. Owing to the inclusion of FA at the expanse of the LFS, as shown by the EDAX analysis, F10 exhibits a comparatively lower calcium content with an increase in aluminum, suggesting the creation of certain geopolymer phases. The microstructure of the sample made from 70% LFS with 30% FA (F30) was completely altered. A number of characteristics have emerged. First, a significant number of small pores are formed, which largely reduces the huge spaces. This was caused by the creation of more geopolymer phases (gel networks). Second, a significant number of long CASH plate grains were found in the microstructure, acting as reinforcements for the geopolymer gel. The apparent porosity may have increased because of the formation of more geopolymer gels with numerous tiny pores (Figure 6b). The improvement in the strength of F30 is due to the long-plate CASH phase reinforcing the geopolymer gel network.

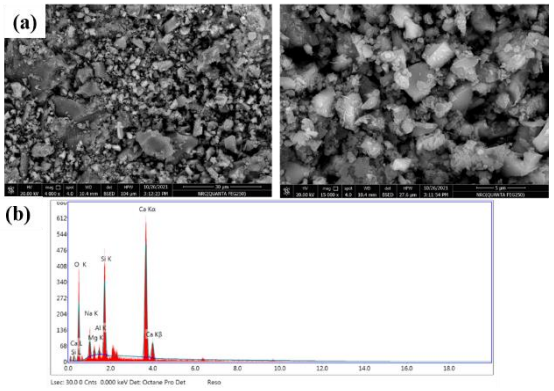

Figure 9 The SEM (a) and EDAX (b) analyses of the geopolymer that was synthesized using 100% slag and cured in air for 28 days.

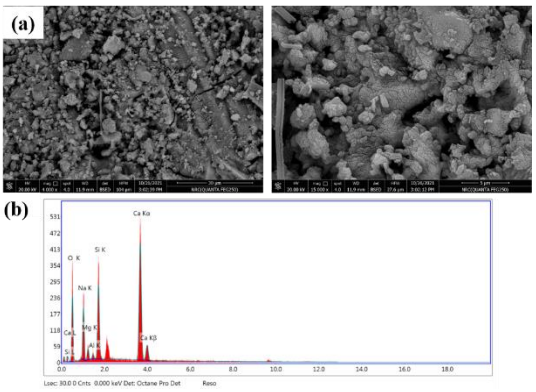

Figure 10 SEM (a) and EDAX (b) analysis results for the geopolymer samples prepared using 10% fly ash and 90% blast furnace slag, which were cured in air for 28 days.

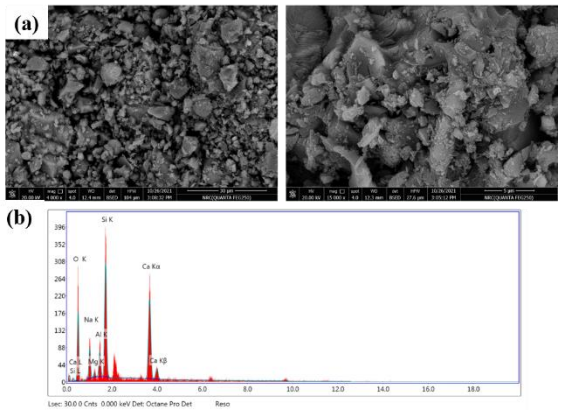

Figure 11 SEM micrographs (a) and EDAX (b) analysis of geopolymer prepared from 30%FA and 70% slag, cured in air for 28-days.

Compression strength of produced geopolymer

Prior to the evaluation of the mechanical properties, the specimens were visually inspected for potential cracks. Provided they are free of cracks, they are relatively large, as shown in Figure 12. Figure 13 shows the compressive strength of the fabricated geopolymers. When 10% FA was added to the ladle slag (batch F10), the compressive strength decreased. However, when 30% FA (batch F30) was added, the compression strength improved and reached a

maximum value of 14.5 MPa. The fluctuation in strength indicates a varying degree of gel formation and the extent of interaction between the LFS and FA, which influences the geopolymer microstructure. The addition of 10% FA resulted in increased porosity, which diminished the compression strength. Conversely, sample F30, which contained 30% FA, exhibited the highest compression strength. This can be attributed to two factors. First, long plate-like grains of CASH phase are formed, serving as the interlocking mechanism for the matrix. Second, only small-sized pores are generated in the geopolymer gel-structure, with fewer large voids present. Although there are numerous small pores, their impact on the value of compression strength is insignificant compared to the large voids that weaken the strength. Therefore, the addition of Ca with an aluminosilicate group either enhances or weakens the mechanical properties of the fabricated geopolymers, based on their ratios and the development of CASH-gel. Evidently, an optimal ratio exists that can yield the best possible strength, as demonstrated by the outcome for F30 sample.

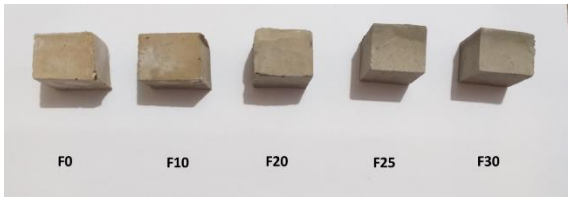

Figure 12 Visual observation of prepared geopolymers cured in air for 28-days.

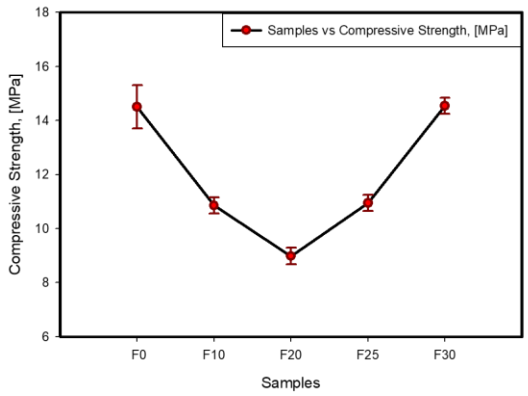

Figure 13 Compressive strength of sunthesized geopolymers cured in air for 28-days, produced at different 100% to 70% LFS.

Biodiesel production in the presence of geopolymer powders

Mono-alkyl esters of long-chain fatty acids derived from renewable vegetables or animal fats, known as biodiesel, are utilized in ignition engines. These fuels are subject to diesel and biodiesel fuel regulations owing to their essential characteristics, including flash point, viscosity, and density [48]. The density of biodiesel is known to vary between 0.848 and 0.885 g/cm^3 at 38°C. This variation in density can affect the performance of the fuel-injection system, resulting in increased viscosity and higher density. For instance, an increase in density from 0.848 to 0.885 g/cm^3 can result in an increase in viscosity from 2.8 to 5.1 centistokes (1 centistokes = 1 mm^2/s) [49]. Kinematic viscosity plays a significant role in the functionality of fuel-injection systems, particularly at lower temperatures. As the viscosity of biodiesel increases, less atomization of the fuel spray occurs, which results in imprecise injection procedures. Reports suggest that the kinematic viscosity of various biodiesels derived from various oils ranges between 2.8 and 5.1 centistokes (cSt) at 38 °C [50]. The flash point indicates the ignition characteristics of a fuel, with higher flash points indicating lower volatility. Biodiesel produces fewer pollutants and exhibits better ignition quality than petroleum-based diesel. It is sulfur-free and has a high flash point. European standard reports the lowest flash point for biodiesel as 101 °C, whereas ASTM D-93 specifies that the flash point of biodiesel must be between 93 and 130 °C. Table 3 displays the density, flash point, and viscosity information for certain biodiesel samples produced with the geopolymer catalyst. The amount of biodiesel produced was determined by the temperature at which the geopolymer catalyst was calcined, with higher temperatures producing more biodiesel than lower temperatures. Figure 14 illustrates the images of the separated biodiesel samples and the selected sample biodiesel (catalyst, biodiesel, and glycerol layers). The data in Table 3 indicate that the density, flash point, and viscosity values of these biodiesel samples fall within the typical range of common biodiesels.

Table 3 Physical properties of chosen biodiesels synthesized via geopolymer catalyst.

Sample	Firing Temp, °C	Density, g/cm^3	Viscosity mm^2/sec	Flash Temp, °C
F0	500	0.87001	4.3906	135
F10	300	0.86210	4.4207	131
F20	700	0.86185	4.4413	132
F25	300	0.86071	4.4617	130
F30	700	0.86142	4.4620	129

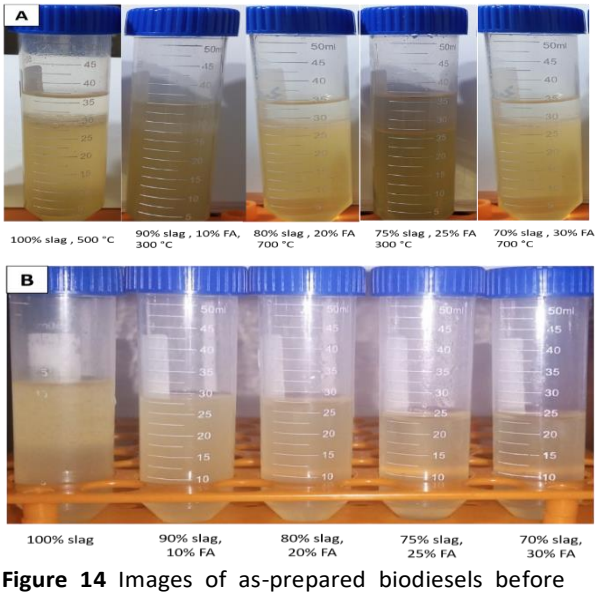

Figure 14 Images of as-prepared biodiesels before separation (A) and separated biodiesel (B).

Conclusions

The following findings were established:

1. As a result, we were able to properly dispose of waste and develop a useful geopolymer catalyst for energy-related applications, particularly in the production of biodiesel.
2. Fly ash and slag from ladle furnaces were successfully combined to create hardened bulk geopolymers with enhanced compressive strengths and physical characteristics. The addition of fly ash to slag resulted in the formation of sodium and calcium aluminum silicate hydrate phases (NASH and CASH, respectively), which improved the properties of the slag.
3. The resulting geopolymer structure's big voids and small pores significantly affect its mechanical and physical properties. The batch with the highest compressive strength (14.5 MPa) consisted of 70% slag and 30% fly ash.
4. The production of biodiesel from methanol and soybean oil is facilitated by the effective calcination of fine geopolymer powders at different temperatures. The generated biodiesel's density, viscosity, and flash point were all within the range of previously well-known biodiesel parameters.

Funding Sources

This research received no external funding.

Conflicts of Interest

There are no conflicts to declare.

Acknowledgements

The authors extend their appreciation to the Suez and Sinai Metallurgical and Materials Research Centre of Scientific Excellence (SSMMR-CSE).

References

[1] El-Sayed Seleman, M. M., El-Kheshen, A. A., Kharbish, S., & Ebrahim, W. R. (2020). Utilization of cement kiln dust for the preparation of borosilicate glass. Interceram. - International Ceramic Review, 69, 26–33. https://doi.org/10.1007/s42411-020-0426-8

[2] Garside, M. (2023). Cement production worldwide from 1995 to 2022. Chemicals & Resources, Mining, Metals & Minerals, Statistics.

[3] Davidovits, J. (2017). Geopolymers: Ceramic-like inorganic polymers. Journal of Ceramic Science and Technology, 8(3), 335-350. https://doi.org/10.4416/jcst2017-00038

[4] Samal, A. K., Panigrahi, M., Ganguly, R. I., & Dash, R. R. (2023). Applications, challenges and opportunities of geopolymer materials. In Development of Geopolymer from Pond Ash-Thermal Power Plant Waste: Novel Constructional Materials for Civil Engineers (Chap. 8). https://doi.org/10.1002/9781394167975.ch8

[5] Ettahiri, Y., Bouargane, B., Fritah, K., Akhsassi, B., Pérez-Villarejo, L., Aziz, A., Bouna, L., Benlhachemi, A., & Novais, R. M. (2023). A state-of-the-art review of recent advances in porous geopolymer: Applications in adsorption of inorganic and organic contaminants in water. Construction and Building Materials, 395, 132269.

[6] El-Sayed Seleman, M. M., El-Kheshen, A. A., Raslan, M. F., & Shoeir, R. H. (2022). Glass production using tailing of upgraded rare metal mineralization, Abu Rusheid area – Egypt for nuclear waste immobilization. Ceramics International, 48, 569-577. https://doi.org/10.1016/j.ceramint.2021.09.135

[7[Gasca-Tirado, J. R., Manzano-Ramírez, A., & Reyes-Araiza, J. L. (2017). The potential use of geopolymer for cleaning air. In Sustainable and Nonconventional Construction Materials Using Inorganic Bonded Fiber Composites (pp. 221-233). https://doi.org/10.1016/B978-0-08-102001-2.000097

[8] Almutairi, A. L., Tayeh, B. A., Adesina, A., Isleem, H. F., & Zeyad, A. M. (2021). Potential applications of geopolymer concrete in construction: A review. Case Studies in Construction Materials, 15, e00733. https://doi.org/10.1016/j.cscm.2021.e00733

[9] Cong, P., & Cheng, Y. (2021). Advances in geopolymer materials: A comprehensive review. Journal of Traffic and Transportation Engineering (English Edition), 8, 283-314. https://doi.org/10.1016/j.jtte.2021.03.004

[10] Kishore, K., Pandey, A., Wagri, N. K., Saxena, A., Patel, J., & Al-Fakih, A. (2023). Technological challenges in nanoparticle-modified geopolymer concrete: A comprehensive review on nanomaterial dispersion, characterization techniques and its mechanical properties. Case Studies in Construction Materials, 19, e02265. https://doi.org/10.1016/j.cscm.2023.e02265

[11] Dheyaaldin, M. H., Mosaberpanah, M. A., & Shi, J. (2023). The effects of nanomaterials on the characteristics of aluminosilicate-based geopolymer composites: A critical review. Journal of Building Engineering, 73, 106713. https://doi.org/10.1016/j.jobe.2023.106713

[12] Das, S. K., Mishra, J., Singh, S. K., Mustakim, S. M., Patel, A., Das, S. K., & Behera, U. (2020). Characterization and utilization of rice husk ash (RHA) in fly ash – Blast furnace slag based geopolymer concrete for sustainable future. Materials Today: Proceedings, 33, 5162-5167.

[13] Sidhu, J., & Kumar, P. (2023). Development of hydrophobicity in geopolymer composites - Progress and perspectives. Construction and Building Materials, 396, 132344.

[14] Nassar, A. K., & Kathirvel, P. (2023). Effective utilization of agricultural waste in synthesizing activator for sustainable geopolymer technology. Construction and Building Materials, 362, 129681. https://doi.org/10.1016/j.conbuildmat.2022.129681

[15] Kaze, R. C., Naghizadeh, A., Tchadjie, L., Adesina, A., Djobo, J. N. Y., Nemaleu, J. G. D., Kamseu, E., Melo, U. C., & Tayeh, B. A. (2022). Lateritic soils based geopolymer materials: A review. Construction and Building Materials, 344, 128157. https://doi.org/10.1016/j.conbuildmat.2022.128157

[16] Shehata, N., Mohamed, O. A., Sayed, E. T., Abdelkareem, M. A., & Olabi, A. G. (2022). Geopolymer concrete as green building materials: Recent applications, sustainable development and circular economy potentials. Science of the Total

Environment, 836, 155577. http://dx.doi.org/10.1016/j.scitotenv.2022.155577

[17] Chen, X., Zhang, J., Lu, M., Chen, B., Gao, S., Bai, J., & Yang, Y. (2022). Study on the effect of calcium and sulfur content on the properties of fly ash based geopolymer. Construction and Building Materials, 314, 125650. https://doi.org/10.1016/j.conbuildmat.2021.125650

[18] Li, J., Dang, X., Zhang, J., Yi, P., & Li, Y. (2023). Mechanical properties of fly ash-slag based geopolymer for repair of road subgrade diseases. Polymers, 15(2). https://doi.org/10.3390/polym15020309

[19] Azad, N. M., & Samarakoon, S. M. S. M. K. (2021). Utilization of industrial by-products/waste to manufacture geopolymer cement/concrete. Sustainability, 13(2), 873. https://doi.org/10.3390/su13020873

[20] Ren, B., Zhao, Y., Bai, H., Kang, S., Zhang, T., & Song, S. (2021). Eco-friendly geopolymer prepared from solid wastes: A critical review. Chemosphere, 267, 128900.

[21] Wardhono, A., Law, D. W., & Strano, A. (2015). The strength of alkali-activated slag/fly ash mortar blends at ambient temperature. Procedia Engineering, 125, 650–656. https://doi.org/10.1016/j.proeng.2015.11.095

[22] Botti, R. F., Innocentini, M. D. M., Faleiros, T. A., Mello, M. F., Flumignan, D. L., Santos, L. K., Franchin, G., & Colombo, P. (2021). Additively manufactured geopolymer structured heterogeneous catalysts for biodiesel production. Applied Materials Today, 23, 101022. https://doi.org/10.1016/j.apmt.2021.101022

[23] Anastas, P. T., Kirchhoff, M. M., & Williamson, T. C. (2001). Catalysis as a foundational pillar of green chemistry. Applied Catalysis A: General, 33(10), 3–13. https://doi.org/10.1016/S0926-860X(01)00793-1

[24] Ramos, M., Dias, A. P. S., Puna, J. F., Gomes, J., & Bordado, J. C. (2019). Biodiesel production processes and sustainable raw materials. Energies, 12. https://doi.org/10.3390/en12234408

[25] Ren, Y., He, B., Yan, F., Wang, H., Cheng, Y., Lin, L., Feng, Y., & Li, J. (2012). Continuous biodiesel production in a fixed bed reactor packed with anion-exchange resin as heterogeneous catalyst. Bioresource Technology, 113, 19–22. https://doi.org/10.1016/j.biortech.2011.10.103

[26] Lianhua, L., Pengmei, L., Wen, L., Zhongming, W., & Zhenhong, Y. (2010). Esterification of high FFA tung oil with solid acid catalyst in fixed bed reactor. Biomass and Bioenergy, 34, 496–499. https://doi.org/10.1016/j.biombioe.2009.12.014

[27] Hernández-Montelongo, R., García-Sandoval, J. P., González-Álvarez, A., Dochain, D., & Aguilar-Garnica, E. (2018). Biodiesel production in a continuous packed bed reactor with recycle: A modeling approach for an esterification system. Renewable Energy, 116, 857–865. https://doi.org/10.1016/J.RENENE.2017.09.030

[28] Wu, H., Zhang, J., Wei, Q., Zheng, J., & Zhang, J. (2013). Transesterification of soybean oil to biodiesel using zeolite-supported CaO as strong base catalysts. Fuel Processing Technology, 109, 13–18. https://doi.org/10.1016/j.fuproc.2012.09.032

[29] Bakkar, A., El-Sayed Seleman, M. M., Zaky Ahmed, M. M., Harb, S., Goren, S., & Howsawi, E. (2023). Recovery of vanadium and nickel from heavy oil fly ash (HOFA): A critical review. RSC Advances, 13, 6327–6345. https://doi.org/10.1039/D3RA00289F

[30] Designation, A. S. T. M. (2003). C618-03,". Standard Specification for Coal Fly Ash and Raw or Calcined Natural Pozzolan for Use in Concrete", Annual Book of ASTM Standards, 319-321.

[31] Ng, H. T., Heah, C. Y., Mold Mustafa Al Bakri, A., Ng, Y. S., & Ridho, B. (2020). Study of fly ash geopolymer and fly ash/slag geopolymer in terms of physical and mechanical properties. European Journal of Materials Science and Engineering, 5, 187–198. https://doi.org/10.36868/ejmse.2020.05.04.187

[32] Farhan, K. Z., Johari, M. A. M., & Demirboğa, R. (2020). Assessment of important parameters involved in the synthesis of geopolymer composites: A review. Construction and Building Materials, 264, 120276. https://doi.org/10.1016/j.conbuildmat.2020.120276

[33] Jiang, X., Zhang, Y., Zhang, Y., Ma, J., Xiao, R., Guo, F., Bai, Y., & Huang, B. (2023). Influence of size effect on the properties of slag and waste glass-based geopolymer paste. Journal of Cleaner Production, 383, 135428. https://doi.org/10.1016/j.jclepro.2022.135428

[34] Zhao, R., Yuan, Y., Cheng, Z., Wen, T., Li, J., Li, F., & Ma, Z. J. (2019). Freeze-thaw resistance of Class F fly ash-based geopolymer concrete. Construction and Building Materials, 222, 474–483. https://doi.org/10.1016/j.conbuildmat.2019.06.166

[35] El Alouani, M., Alehyen, S., El Achouri, M., Hajjaji, A., Ennawaoui, C., & Taibi, M. H. (2020). Influence of the nature and rate of alkaline activator on the physicochemical properties of fly ash-based geopolymers. Advances in Civil Engineering, 2020, 8880906. https://doi.org/10.1155/2020/8880906

[36] Richardson, I. G. (1999). The nature of CSH in hardened cements. Cement and Concrete Research, 29(8), 1131–1147. https://doi.org/10.1016/S0008-8846(99)00168-4

[37] Richardson, I. G., Brough, A. R., Groves, G. W., & Dobson, C. M. (1994). The characterization of hardened alkali-activated blast-furnace slag pastes and the nature of the calcium silicate hydrate (CSH) phase. Cement and Concrete Research, 24(5), 813–829. https://doi.org/10.1016/0008-8846(94)90002-7

[38] Taylor, H. F. (1997). Cement chemistry. Thomas Telford.

[39] Renaudin, G., Russias, J., Leroux, F., Cau-dit-Coumes, C., & Frizon, F. (2009). Structural characterization of C–S–H and C–A–S–H samples—part II: Local environment investigated by spectroscopic analyses. Journal of Solid State Chemistry, 182(12), 3320–3329. https://doi.org/10.1016/j.jssc.2009.09.024

[40] Provis, J. L., & van Deventer, J. S. J. (2009). Geopolymers: Structures, processing, properties and industrial applications. Elsevier.

[41] Sunarsih, E. S., As'ad, S., Sam, A. R. M., & Kristiawan, S. A. (2023). Properties of fly ash-slag-based geopolymer concrete with low molarity sodium hydroxide. Civil Engineering Journal, 9(2). http://dx.doi.org/10.28991/CEJ-2023-09-02-010

[42] Yusuf, M. O. (2023). Bond characterization in cementitious material binders using Fourier-transform infrared spectroscopy. Applied Sciences, 13(5), 3353. https://doi.org/10.3390/app13053353

[43] Srinivasamurthy, L., Chevali, V. S., Zhang, Z., & Wang, H. (2023). Effect of fly ash to slag ratio and Na2O content on leaching behaviour of fly ash/slag-based alkali-activated materials. Construction and Building

Materials, 383, 131234. https://doi.org/10.1016/j.conbuildmat.2023.131234

[44] Lao, J. C., Huang, B. T., Fang, Y., Xu, L. Y., Dai, J. G., & Shah, S. P. (2023). Strain-hardening alkali-activated fly ash/slag composites with ultra-high compressive strength and ultra-high tensile ductility. Cement and Concrete Research, 165, 107075. https://doi.org/10.1016/j.cemconres.2022.107075

[45] Guo, H., Yuan, P., Zhang, B., Wang, Q., Deng, L., & Liu, D. (2021). Realization of high-percentage addition of fly ash in the materials for the preparation of geopolymer derived from acid-activated metakaolin. Journal of Cleaner Production, 285, 125430. https://doi.org/10.1016/j.jclepro.2020.125430

[46] Hoyos-Montilla, A. A., Puertas, F., Mosquera, J. M., & Tobón, J. I. (2022). Infrared spectra experimental analyses on alkali-activated fly ash-based binders. Spectrochimica Acta Part A: Molecular and Biomolecular Spectroscopy, 269, 120698. https://doi.org/10.1016/j.saa.2021.120698

[47] Lv, Q., Yu, J., Ji, F., Gu, L., Chen, Y., & Shan, X. (2021). Mechanical property and microstructure of fly ash-based geopolymer activated by sodium silicate. KSCE Journal of Civil Engineering, 25(5), 1765–1777.

[48] Alptekin, E., & Canakci, M. (2008). Determination of the density and the viscosities of biodiesel–diesel fuel blends. Renewable Energy, 33, 2623–2630. https://doi.org/10.1016/j.renene.2008.02.020

[49] Alsultan, A. G., Asikin-Mijan, N., Ibrahim, Z., Yunus, R., Razali, S. Z., Mansir, N., Islam, A., Seenivasagam, S., & Taufiq-Yap, Y. H. (2021). A short review on catalyst, feedstock, modernized process, current state, and challenges on biodiesel production. Catalysts, 11(11), 1261. https://doi.org/10.3390/catal11111261

[50] Barbarey, M. S., El-Sayed Seleman, M. M., El Kheshen, A. A., & Zawrah, M. F. (2024). Utilization of ladle furnace slag for fabrication of geopolymer: Its application as catalyst for biodiesel production. Construction and Building Materials, 411, 134226. https://doi.org/10.1016/j.conbuildmat.2023.134226